Globular clusters in dwarf galaxies as probes of dark matter

M2 Internship Report

LIRA - Observatoire de Paris
March 16 – July 10, 2026

Intern: Maxime ASSUERUS
Supervisor: Pierre BOLDRINI (`Pierre.Boldrini@obspm.fr`),
Affiliation: `https://lira.observatoiredeparis.psl.eu/`

Abstract

Globular clusters in dwarf galaxies are valuable tracers of the underlying dark matter distribution, since their orbital evolution is strongly affected by dynamical friction. This process depends on the local density of matter surrounding the cluster, and is therefore particularly sensitive to the presence and distribution of dark matter in dwarf galaxies. In the standard cold dark matter framework, this friction can be efficient enough to make globular clusters spiral toward the centre of their host galaxy within a few Gyr. However, several dwarf galaxies still host globular clusters at large galactocentric radii, leading to the so-called globular cluster timing problem.

In this report, we investigate whether the shape of the dark matter potential can affect the infall time of globular clusters and therefore help resolve this tension. We use the `TNG50` cosmological simulation to estimate the typical shapes of dwarf galaxy dark matter halos. We find that dwarf galaxy halos are generally non-spherical, with typical global axis ratios around $b \sim 0.75$ and $c \sim 0.85$, and with substantial halo-to-halo scatter.

We first model dwarf galaxies using analytical NFW-like dark matter potentials implemented in `galpy`, ranging from spherical to flattened configurations. We integrate globular cluster orbits including Chandrasekhar dynamical friction and show that non-spherical halos can significantly delay orbital decay. In particular, flattened potentials increase the infall time compared to the spherical case, with the effect depending on both the halo axis ratio and the initial orbital orientation.

We then define a critical initial radius, $r_{\text{init,crit}}$, corresponding to the maximum radius from which a globular cluster can reach the central region within 10 Gyr. This provides a quantitative way to assess the survival of globular clusters in different halo geometries. Our results show that the critical radius depends strongly on the halo shape and mass, indicating that the timing problem cannot be fully assessed using spherical models alone.

Overall, this work shows that dark matter halo geometry is an important ingredient in the orbital evolution of globular clusters. Non-spherical potentials can lengthen globular cluster survival times and may therefore contribute to reducing the severity of the globular cluster timing problem in dwarf galaxies.

Acknowledgements

First of all, I would like to thank Dr. Pierre BOLDRINI, my internship tutor, who was with me throughout my internship. He always took the time to answer my questions and help me. I really enjoyed talking to him about my internship topic. Finally, I'd like to thank the "Stars and Galaxies" LIRA (Observatoire de Paris) team for the warm welcome they gave me.

Contents

1 Introduction

Dark matter (DM) remains one of the greatest unresolved problems in modern astrophysics. At present, the ΛCDM model is the standard cosmological framework used to describe the evolution of the Universe and its mass-energy content. The most precise observations indicate that, for a flat Universe, the total mass-energy budget is dominated by matter, $\Omega_\mathrm{m} = 0.315 \pm 0.007$, and dark energy, $\Omega_\Lambda = 0.685 \pm 0.007$ (see N. and Aghanim et al. (2020) [1]). The matter density parameter, Ω_m, includes both baryonic matter and dark matter. These measurements confirm that baryonic matter accounts for only 4.9% of the total mass-energy content of the Universe. However, the physical nature of dark matter remains unknown and is still an active area of research.

Cosmological simulations based on the ΛCDM paradigm show that dark matter clusters into gravitationally bound structures known as dark matter halos. The density distribution of these halos is well described by the Navarro-Frenk-White (NFW) profile [11].

The ΛCDM model has been remarkably successful in describing the physics of the Universe on cosmological scales. Its predictions have been extensively tested through numerical simulations and are in very good agreement with a wide range of observational data. However, on smaller scales, particularly at galactic scales (1–100 kpc), several tensions with observations remain. For example, the cuspy central density profiles predicted for dark matter halos, a characteristic feature of the NFW profile, are often not supported by observations (see Oh et al. 2011 [12]). In this work, we focus on another discrepancy related to dynamical friction (DF).

First derived by Chandrasekhar in 1943 [5], dynamical friction is a fundamental physical process in galaxies that governs the orbital decay of massive objects such as black holes, satellite galaxies, and globular clusters (GCs). As a massive body moves through a background medium, it creates a gravitational wake, that is, an overdensity trailing behind it, which exerts a drag force and causes the object to lose energy and slow down.

Globular clusters are gravitationally bound, approximately spherical stellar systems orbiting within galaxies (see Figure 12). They typically contain between 10^4 and 10^6 stars. As they move through dark matter halos of galaxies, their dynamics are expected to be significantly influenced by dynamical friction (see Figure 13). Globular clusters are important astrophysical systems for several reasons. In particular, they provide valuable constraints on the age of the Universe, since they are among the oldest known stellar systems and typically have ages exceeding 10 Gyr. Their high degree of compactness makes them relatively resistant to tidal disruption, which explains their long-term survival. Nevertheless, their formation mechanism remains poorly understood. In dwarf galaxies, tidal effects are expected to be negligible, making globular clusters especially useful tracers of the underlying gravitational potential.

The predicted dynamical friction of the CDM model is too strong in some cases. Let us illustrate this with the example of the Fornax dwarf galaxy and its "timing problem" (see Meadows , Noah et al. (2020) [10], for example). Assuming CDM dynamical friction, Fornax should have disrupted its GCs, and this is not what we observe. The globular cluster timing problem is not restricted to the Fornax dwarf spheroidal galaxy and may also be relevant for a wider population of nearby dwarf galaxies that are now being explored with recent surveys such as *Euclid* (see Boldrini et al. 2026 in prep). Several possible explanations may account for these discrepancies. One possibility is that the merger history of dwarf galaxies plays an important role, since past interactions can modify the orbits of globular clusters (see Leung et al. 2019 [9]). Another possibility is that some globular clusters may have formed inside their own dark matter mini-halos (see Boldrini et al. 2020 [3]). In this scenario, the cluster would not initially be a purely stellar system, but would be embedded in a small dark matter subhalo. This could modify its early orbital evolution, its effective mass, and its response to dynamical friction, potentially affecting the predicted infall time. Alternatively, it is also likely that the answer is hidden in the DM nature.

The aim of this work is to investigate how the shape of the dark matter potential in a dwarf galaxy can affect the infall time of globular clusters (GCs). To this end, we construct an ellipsoidal dark matter potential based on an initially spherical NFW profile.

The report is organized as follows. We first introduce the motivation behind the globular cluster timing problem. We then turn to the `TNG50` cosmological simulation in order to estimate the typical shapes of dark matter halos associated with dwarf galaxies and to assess whether non-spherical halo geometries are expected in a realistic cosmological context. After this, we present the theoretical description of dynamical friction and the numerical methodology used to integrate globular cluster orbits in analytical dark matter potentials. The following sections study the effect of halo geometry on globular cluster infall and compare the model with previous results from the literature.

2 Motivation

The motivation for this work comes from the globular cluster timing problem. This issue is not limited to Fornax galaxy, but may affect a broader population of nearby dwarf galaxies, as recent observations from the *Euclid* survey appear to suggest. The *Euclid* mission is a space telescope launched by the European Space Agency to study the dark Universe, in particular dark matter and dark energy. Its main goal is to map the large-scale structure of the Universe by observing billions of galaxies over more than one third of the sky. Although *Euclid* is primarily designed for cosmology, its depth, spatial resolution, and wide sky coverage also make it very useful for studying nearby systems, such as dwarf galaxies and their globular cluster populations. In this context, *Euclid* can provide new samples of globular clusters and their projected distances from the centres of dwarf galaxies.

In particular, Figure 1 shows the orbital decay of 17 globular clusters hosted by different dwarf galaxies in the Fornax galaxy cluster, integrated over 10 Gyr. These objects are precisely the clusters for which a timing problem arises: in the spherical NFW model, dynamical friction predicts that they should have already spiralled into the central regions of their host galaxies. However, they are observed at larger galactocentric distances, suggesting that the standard spherical model may overestimate the efficiency of orbital decay. Each coloured curve corresponds to one globular cluster and shows its galactocentric radius as a function of time. The black dashed line marks the adopted central threshold, $r_{\mathrm{merge}} = 0.2$ kpc. All clusters in this example eventually reach the central region, but their infall times vary significantly from one system to another. The fact that some observed clusters are still found at large radii despite such predicted decay is the essence of the globular cluster timing problem.

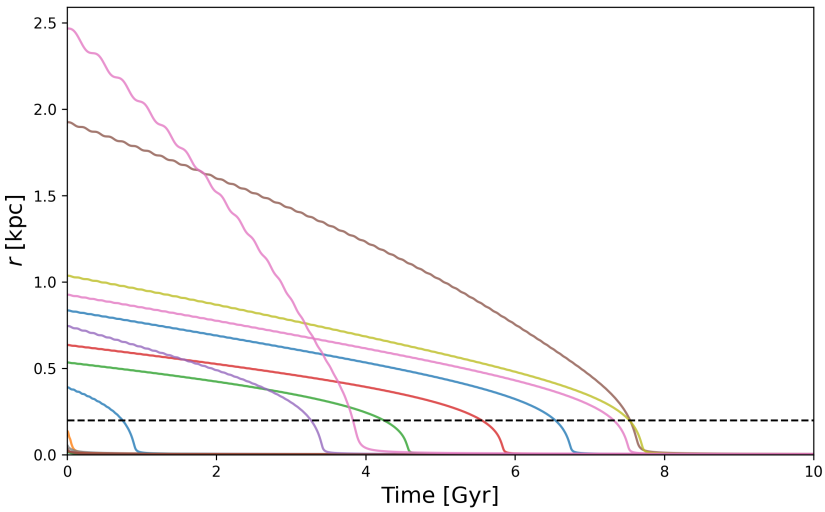

Figure 1: Orbital decay of 17 globular clusters identified in *Euclid* dwarf galaxy candidates in the Fornax galaxy cluster. Each orbit is integrated in a spherical NFW dark matter potential including dynamical friction. The curves show the galactocentric radius as a function of time, illustrating that the clusters fall toward the central region on different timescales.

3 Cosmological simulation TNG50

Before studying the orbital decay of globular clusters in idealized analytical potentials, we first use cosmological simulations to estimate the typical shapes of dark matter halos associated with dwarf galaxies. This provides a realistic motivation for the non-spherical halo geometries that will be explored later in the theoretical part of this report. This step is important because observations generally do not provide direct access to the three-dimensional shape of the dark matter halo. For example, surveys such as *Euclid* can reveal dwarf galaxies and their globular cluster populations, and can provide projected positions, luminosities, and structural properties, but the underlying dark matter halo geometry remains difficult to infer directly from observations alone.

Cosmological simulations offer a complementary approach, since the full phase-space distribution of dark matter particles is known. They therefore allow us to measure the three-dimensional shape of simulated dark matter halos directly and to compare these shapes with the idealized geometries used in the theoretical part of this work. Using the `TNG50` simulation, our goal is to determine whether the halo geometries explored in the theoretical study are representative of realistic dwarf galaxy halos, and to quantify the distribution of dark matter axis ratios in a cosmological sample.

The dwarf galaxy data were extracted from the IllustrisTNG project, a suite of cosmological magnetohydrodynamical simulations of galaxy formation. These simulations follow the joint evolution of dark matter, gas, stars, and black holes in a cosmological volume, starting from early-Universe initial conditions. They are therefore well suited to study the connection between dark matter halos and the galaxies that form within them.

In this work, we use the `TNG50` run because it combines a relatively small cosmological volume with high mass and spatial resolution. This makes it particularly useful for studying low-mass systems such as dwarf galaxies, while still providing a statistically meaningful sample of halos formed in a realistic cosmological environment. It follows the evolution of a cubic cosmological volume of side length

$$L_{\mathrm{box}} \simeq 51.7 \text{ Mpc}$$

The dark matter particle mass in `TNG50` is

$$m_{\mathrm{DM}} = 4.5 \times 10^5\, M_\odot.$$

This high mass resolution makes `TNG50` particularly well suited for studying the internal dark matter structure of low-mass galaxies. We focus on dwarf galaxies. For each selected galaxy, we retrieve a cutout containing only the dark matter particle coordinates. The projected spatial distribution of these particles is then shown in the (x, y) plane as a scatter plot, providing a first visual inspection of the morphology and spatial extent of the dark matter halo for one galaxy (see Figure 2).

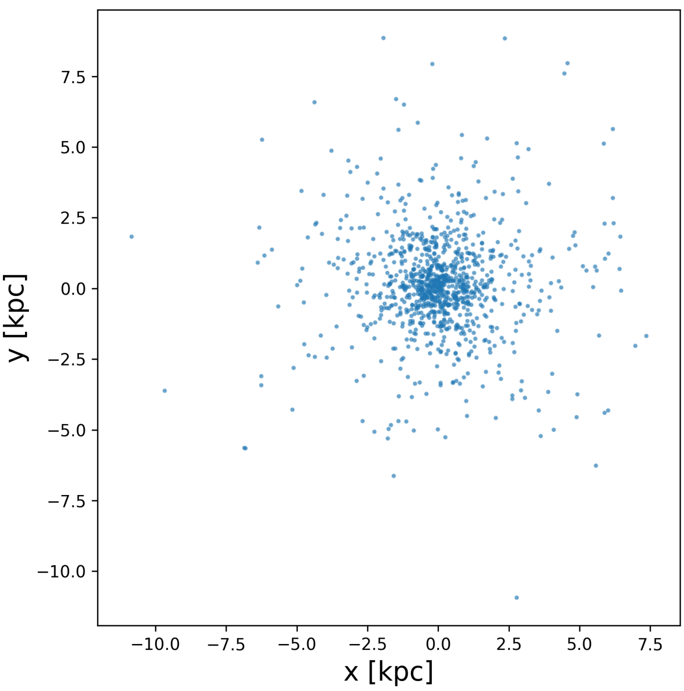

Figure 2: Projected distribution of dark matter particles associated with one TNG50 dwarf galaxy at $z = 0$. This visualization illustrates the spatial extent and morphology of the dark matter component used to measure the global halo shape.

3.1 Shape measurement method

In order to measure the three-dimensional shape of the dark matter halos in the `TNG50` simulation, we use the positions of the dark matter particles associated with each dwarf galaxy. The shape measurement is performed with the `CosmicProfiles` package, which estimates the principal axes of the particle distribution through an iterative ellipsoidal fitting procedure.

The basic idea is to describe the distribution of particles by a shape tensor. For a set of particles with positions $\mathbf{x}_i = (x_i, y_i, z_i)$, the tensor can be written schematically as

$$S_{ij} = \frac{1}{M} \sum_k m_k x_{k,i} x_{k,j},$$

where m_k is the particle mass, $M = \sum_k m_k$, and i, j denote the spatial coordinates. This tensor is the second moment of the mass distribution divided by the total mass: it describes how the particle distribution is spread along different directions.

The tensor is then diagonalized. Its eigenvectors define the principal directions of the best-fitting ellipsoid, while its eigenvalues are related to the axis ratio. If the eigenvalues are ordered as

$$\lambda_1 \geq \lambda_2 \geq \lambda_3,$$

then the corresponding axes satisfy

$$x \propto \lambda_1, \qquad z \propto \lambda_2, \qquad y \propto \lambda_3,$$

where x, z, and y are respectively the major, intermediate, and minor axes of the ellipsoid.

The axis ratios are therefore defined as

$$b = \frac{y}{x} = \frac{\lambda_3}{\lambda_1}, \qquad c = \frac{z}{x} = \frac{\lambda_2}{\lambda_1}.$$

By construction,

$$0 < b \leq c \leq 1.$$

A spherical distribution has $\lambda_1 \simeq \lambda_2 \simeq \lambda_3$, and therefore $b \simeq c \simeq 1$. A flattened or elongated distribution has one eigenvalue significantly smaller than the others, leading to $b < 1$. We use the global shape rather than the local shape profile because our goal is to compare the overall halo geometry with the idealized elliptical potentials used in the orbital integrations (see Section 6).

3.2 Validation on artificial NFW halos

In order to verify that the shape measurement method correctly recovers imposed axis ratios, we generated artificial particle distributions following a NFW profile (see Figure 16). The profile is defined by a scale radius $r_s = 1.36$ kpc, and particles are generated up to a maximum radius $r_{\max} = 30$ kpc. The number of particles used in this test is $N = 10^4$. The particle radii are sampled from the cumulative NFW mass profile (see Navarro et al. (1997) [11]),

$$M(< x) \propto \ln(1 + x) - \frac{x}{1 + x}, \qquad x = \frac{r}{r_s}.$$

We first draw a random variable u uniformly in the interval $[0, 1]$, and then numerically invert the normalized cumulative mass function to obtain the corresponding radius r. The angular directions are sampled isotropically, which produces a spherical NFW particle distribution.

To generate an ellipsoidal halo, the spherical distribution is rescaled along its axes according to

$$X = X, \qquad Y = bY, \qquad Z = cZ.$$

For the test presented here, we choose

$$b = 0.6, \qquad c = 1.0.$$

Both the spherical and ellipsoidal artificial distributions are then analysed with `CosmicProfiles`, using the same procedure as described in Section 3.1. This allows us to check whether the pipeline recovers the expected values of b and c before applying it to the simulated dwarf galaxies.

We also verify that the generated particle distribution reproduces the imposed NFW density profile. For this purpose, the three-dimensional density profile is reconstructed by counting particles in radial shells. The density in each shell is estimated as

$$\rho \simeq \frac{N_{\rm shell}}{V_{\rm shell}}.$$

For an ellipsoidal shell, the volume is

$$V_{\rm shell} = \frac{4\pi}{3} bc \left(m_{\rm out}^3 - m_{\rm in}^3\right),$$

where m is the ellipsoidal radius,

$$m = \sqrt{x^2 + \left(\frac{y}{b}\right)^2 + \left(\frac{z}{c}\right)^2}.$$

The measured profile is then compared to the theoretical NFW profile. Figure 17 confirms that the sampling procedure reproduces the imposed NFW radial profile in spherical and elliptical cases before the artificial distribution is used to test the shape measurement.

To test the robustness of the shape measurement, we generated artificial NFW halos with different numbers of particles, ranging from $N = 100$ to $N = 10^5$. For each value of N, we measured the axis ratios as described before. For the spherical halo, the expected values are

$$c = 1, \qquad b = 1.$$

For the ellipsoidal halo, the expected values are

$$c \simeq 1, \qquad b \simeq 0.6.$$

Figure 3 show that the shape measurement is strongly affected by particle noise when the number of particles is small, especially for

$$N \lesssim 10^3.$$

As N increases, the measured axis ratios progressively converge toward the imposed values. The red horizontal lines in the figure indicate 90% of the expected values and are used as a visual threshold for convergence. This test shows that using at least $N \sim 1000$ particles provides a reasonable compromise between numerical reliability and sample size. We therefore adopt $N_{\rm DM} > 1000$ as a minimum resolution criterion for the shape analysis of TNG dwarf galaxy halos.

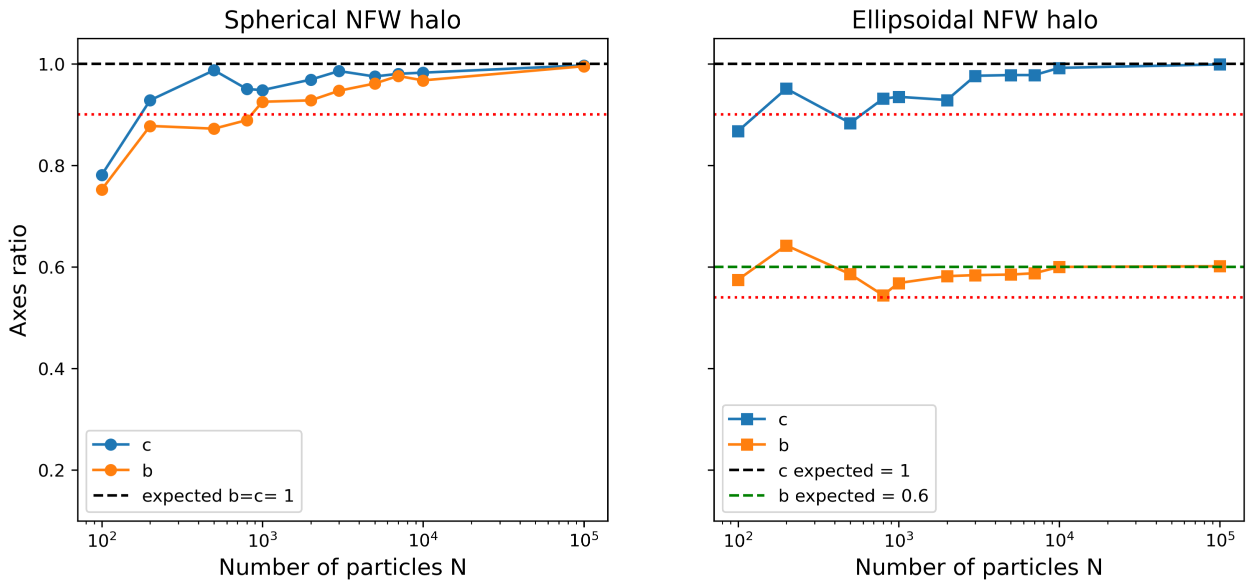

Figure 3: Convergence test of the shape measurement as a function of the number of particles N. The left panel shows the axis ratios measured for a spherical NFW halo, for which the expected values are $b = 1$ and $c = 1$. The right panel shows the corresponding test for an ellipsoidal NFW halo, constructed with axes proportional to $1 : 0.6 : 1$, for which the expected values after axis reordering are $c \simeq 1$ and $b \simeq 0.6$. The horizontal dashed lines indicate the expected values, while the red dotted lines mark 90% of the corresponding expected ratios. The measurements become increasingly stable as N grows, showing that halos with $N \gtrsim 10^3$ particles provide a reasonable compromise between accuracy and sample size.

3.3 Application to TNG50 dwarf galaxies

After validating the shape-measurement pipeline on controlled artificial halos, we apply it to the TNG50 dwarf galaxy sample. This allows us to quantify the distribution of halo shapes in a cosmological context and to test whether the measured axis ratios depend on the dark matter halo mass. To investigate a possible dependence of the TNG halo shapes on mass, we fitted the measured axis ratios as a function of the dark matter mass $M_{\rm DM}$. We restrict the analysis to halos containing more than 1000 dark matter particles, in order to ensure a minimum numerical resolution (see Section 3.2). The dark matter mass is estimated from the number of particles as

$$M_{\rm DM} = N_{\rm DM}\, m_{\rm DM},$$

where, for `TNG50`, $m_{\rm DM} \simeq 4.5 \times 10^5\, M_\odot$.

We fit a linear relation as a function of logarithmic mass:

$$b = a_1 + b_1 \left[\log_{10}\left(\frac{M_{\rm DM}}{M_\odot}\right) - 10 \right],$$

and similarly for c:

$$c = a_2 + b_2 \left[\log_{10}\left(\frac{M_{\rm DM}}{M_\odot}\right) - 10 \right].$$

The subtraction of 10 corresponds to choosing a pivot mass of $10^{10} M_\odot$. With this convention, a_1 and a_2 can be directly interpreted as the typical values of b and c at $M_{\rm DM} = 10^{10} M_\odot$.

The fit is performed by maximizing a Gaussian likelihood, including an intrinsic scatter term $\sigma_{\rm int}$. The total variance used in the likelihood is

$$\sigma_{\rm tot}^2 = y_{\rm err}^2 + \sigma_{\rm int}^2,$$

where y denotes either b or c. Since individual uncertainties on the measured axis ratios are not available, we adopt a small constant error term, while the physical halo-to-halo scatter around the mean relation is absorbed by $\sigma_{\rm int}$.

The uncertainties on the fitted parameters are estimated using bootstrap resampling. At each bootstrap iteration, a new sample of dwarf galaxies is drawn with replacement from the original catalog, and the relation is refitted. This procedure is repeated 10^4 times. The reported uncertainties correspond to the 16th and 84th percentiles of the bootstrap distributions, equivalent to a 68% confidence interval.

The sample used here consists of dwarf galaxies located within a galaxy cluster in the `TNG50` simulation. The initial catalog contains approximately 800 dwarf galaxies. Applying the resolution cut $N_{\mathrm{DM}} > 1000$ removes about one hundred poorly resolved objects, leaving a final statistical sample of roughly 700 dwarf galaxies.

The best-fitting parameters are summarized in Table 3 and figure 4 shows the global axis ratios of the dark matter density distribution of TNG50 dwarf galaxies as a function of their dark matter mass. The left panel shows the minor-to-major axis ratio b, while the right panel shows the intermediate-to-major axis ratio c. Each blue point corresponds to one dwarf galaxy halo. The red line gives the best-fitting linear relation in $\log_{10}(M_{\mathrm{DM}})$, and the shaded region corresponds to the 68% bootstrap uncertainty on this relation.

The measured values show a large halo-to-halo scatter. Most halos have $b \sim 0.65 - 0.9$ and $c \sim 0.75 - 0.95$, indicating that the dark matter distributions are generally non-spherical but not extremely flattened.

The best-fitting trends are weakly decreasing with mass for both b and c. This suggests that, within this sample, more massive dwarf galaxy halos may be slightly more elongated or flattened. However, the intrinsic scatter is much larger than the fitted trend, and the bootstrap confidence band remains narrow only because of the large number of halos in the sample. Therefore, the main result is not a strong mass dependence, but rather that TNG50 dwarf galaxy dark matter halos typically have global axis ratios around $b \sim 0.75$ and $c \sim 0.85$, with substantial object-to-object variation.

This result is useful for the theoretical part of the work because it gives a cosmological motivation for exploring non-spherical potentials.

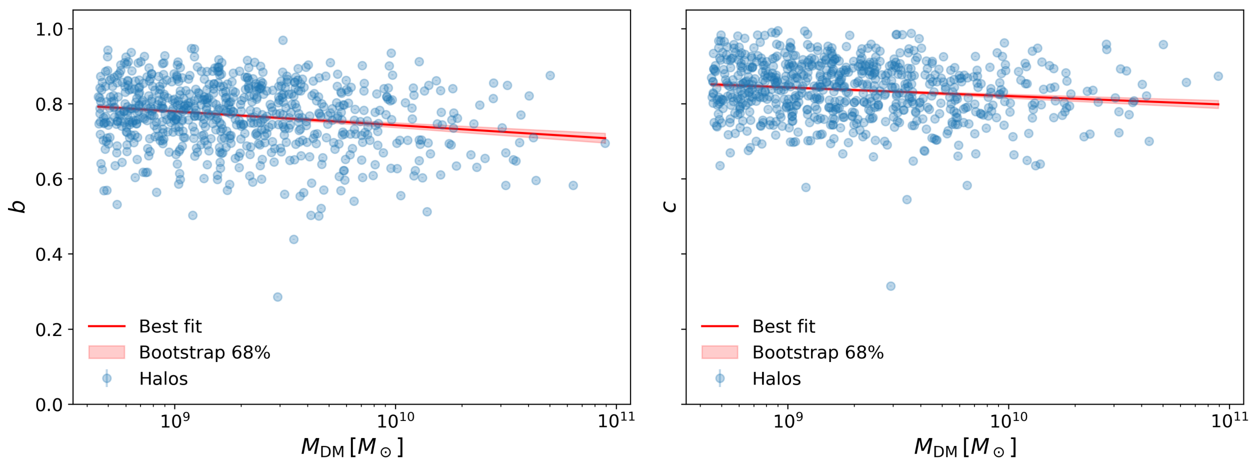

Figure 4: Axis ratios of TNG dwarf galaxy dark matter density as a function of dark matter halo mass, as measured with `CosmicProfiles`. Only halos with more than 1000 dark matter particles are included. The left panel shows the minor-to-major axis ratio b, while the right panel shows the intermediate-to-major axis ratio c. Blue points correspond to roughly 700 individual halos. The red solid line shows the best-fitting linear relation in $\log_{10}(M_{\mathrm{DM}})$, and the shaded red region indicates the 68% confidence interval estimated from bootstrap resampling.

Since the key mechanism driving the orbital decay of GCs is dynamical friction, we now turn to its theoretical description and discuss how it is usually modeled.

4 Dynamical Friction in dark matter halos

Dynamical friction is a fundamental mechanism of energy loss in galactic dynamics, particularly for massive objects such as star clusters, black holes, satellite galaxies, and globular clusters. Let us consider an object of mass $M_{\rm obj}$ orbiting within a gravitational potential of dark matter particles of mass m_{DM} and stellar particles of mass $m_\star$. In the regime where $M_{\rm obj} \gg m_\star$, for example for a globular cluster ($M_{\rm obj} \sim 10^6\, M_\odot$) orbiting within a galaxy, the massive object significantly deviates the surrounding field particles along its trajectory. It results from the combined effect of many encounters of the massive object with other bodies (typically dark matter or stellar particles) in the background distribution. This occurs because, locally, the gravitational force exerted by the massive object dominates over that of the host galaxy. As a result, an overdensity of stars and dark matter forms in its wake, that is, behind the moving object. This gravitational wake exerts a net force opposite to the direction of motion, thereby producing a deceleration (see Figure 13).

Over time, this process causes the orbiting object to lose orbital energy and gradually spiral toward the center of the galactic potential. This phenomenon is known as dynamical friction.

The dynamical friction force derived by Chandrasekhar (1943) (see [5]), under the assumption of a Maxwellian velocity distribution, can be written as

$$\vec{F}_{\rm DF} = -4\pi G^2 M_{\rm obj}^2 \rho(r)\, \frac{\vec{v}}{v^3}\, \ln\Lambda \left[\mathrm{erf}\left(\frac{v}{\sqrt{2}\sigma}\right) - \sqrt{\frac{2}{\pi}}\, \frac{v}{\sigma}\, \exp\left(-\frac{v^2}{2\sigma^2}\right) \right], \tag{1}$$

where the Coulomb logarithm is defined as

$$\ln\Lambda = \ln\left(\frac{r}{\max(r_{\rm hm},\, b_{\rm min})}\right). \tag{2}$$

where $\rho(r)$ is the local mass density of the background medium, here the dark matter halo, evaluated at the position of the orbiting object. The quantity σ is the one-dimensional velocity dispersion of the background particles, which enters through the assumption that their velocities follow an isotropic Maxwellian distribution. This assumption is appropriate for a spherical potential, but it becomes less accurate in an elliptical potential, where the velocity dispersion can be anisotropic and direction-dependent. In such a case, describing the background with a single scalar σ is only an approximation. The Coulomb logarithm is denoted by $\ln\Lambda$, where r is the radial position of the orbiting object and

$$b_{\rm min} = \frac{GM_{\rm obj}}{v^2}$$

is the characteristic impact parameter associated with a 90° deflection. The quantity $r_{\rm hm}$ is the half-mass radius of the object, typically of the order of 10 pc for globular clusters. Finally, v denotes the velocity of the object, $M_{\rm obj}$ its mass, and G the gravitational constant.

As expected, the dynamical friction force is directed opposite to the velocity vector, which reflects its decelerating nature. Its amplitude is proportional to both the mass of the orbiting object and the local density of the host system, implying that dynamical friction is more effective for massive objects moving through denser environments like dwarf galaxies.

The dependence on the Coulomb logarithm also shows that, for a fixed object mass, increasing the size of the object tends to reduce the dynamical friction force, since the denominator involves $r_{\rm hm}$. Physically, dynamical friction is less efficient for extended objects because their mass is distributed over a larger volume, leading to a less concentrated gravitational wake.

Let us consider an example to illustrate the effect of dynamical friction on globular clusters. We model the host dwarf galaxy with a Navarro–Frenk–White (NFW) dark matter halo [11]. The NFW profile is a standard analytical description of dark matter halos formed in cosmological simulations. It is characterized by a cuspy central density profile and by a density that decreases approximately as r^{-3} at large radii. In this example, the halo has a mass $M_{\rm halo} = 10^9\, M_\odot$, a scale radius $r_s = 1.36\,\mathrm{kpc}$, and a virial radius $r_{\rm vir} = 25.66\,\mathrm{kpc}$. The scale radius r_s marks the transition between the inner and outer regimes of the density profile. The corresponding density profile is given by

$$\rho_{NFW}(r) = \frac{M_{\rm halo}}{A_{\rm NFW}\, 4\pi r_s^3 \left(\frac{r}{r_s}\right)\left(1+\frac{r}{r_s}\right)^2}, \tag{3}$$

where

$$A_{\rm NFW} = \ln(1 + c_{vir}) - \frac{c_{vir}}{1 + c_{vir}}, \quad (4)$$

and

$$c_{vir} = \frac{r_{\rm vir}}{r_s} \quad (5)$$

is the concentration parameter. The model considers a globular cluster of mass $M_{\rm gc} = 10^6\,M_\odot$ and half-mass radius $r_{\rm hm,gc} = 10\,\rm pc$, initially placed at a galactocentric distance $R_0 = 2\,\rm kpc$, with an initial vertical position $z_0 = 0\,\rm kpc$ and an initial vertical velocity $v_{z,0} = 0\,\rm km\,s^{-1}$ The initial orbit is chosen to be circular, with eccentricity $e = 0$, and the initial tangential velocity $v_{T,0}$ is set from the circular velocity of the spherical model, such that $v_{T,0} = v_{\rm circ,sph}(R_0)\sqrt{1+e}$, corresponding to a value of the order of $20\,\rm km\,s^{-1}$.

The orbital evolution is then integrated over a timespan of 10 Gyr, comparing cases without dynamical friction to cases including a Chandrasekhar dynamical friction force (see Figure 5). Without dynamical friction, the globular cluster remains on a stable orbit with an almost constant radius around the galaxy centre. When dynamical friction is included, the orbit progressively loses energy and angular momentum, causing the cluster to spiral inward and reach the central region after approximately 4 Gyr.

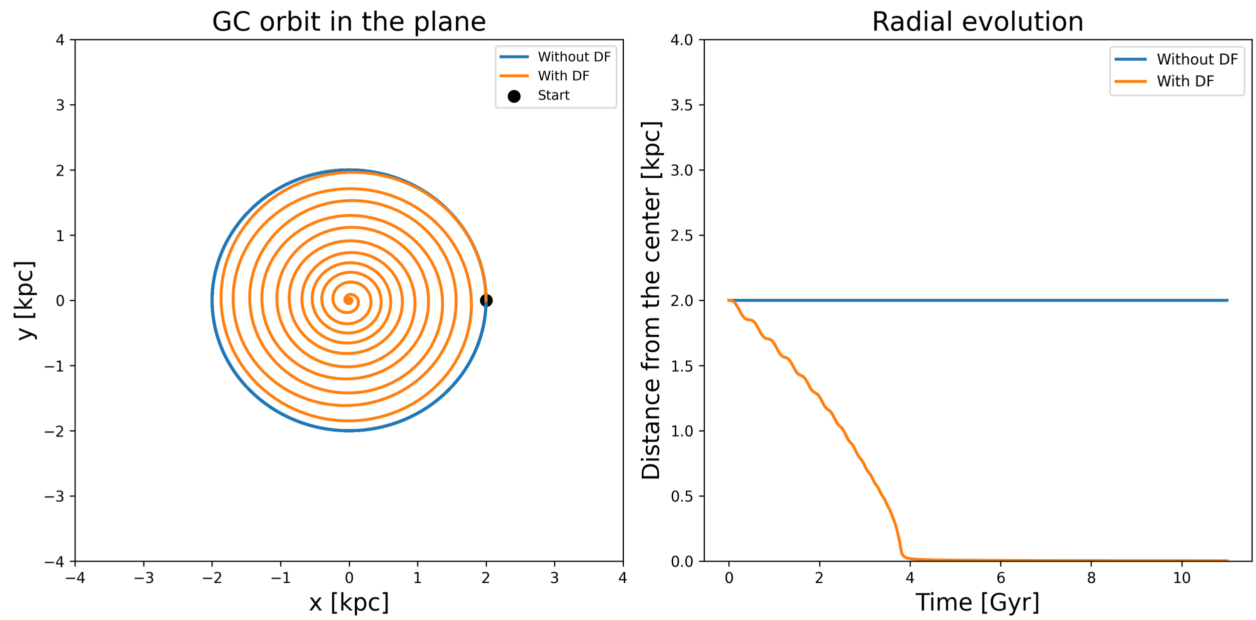

Figure 5: Example of an orbit integration for a globular cluster in a spherical NFW dark matter potential. The left panel shows the trajectory in the orbital plane, comparing the case without dynamical friction and the case including dynamical friction. Without dynamical friction (blue curve), the cluster remains on a stable orbit, while dynamical friction causes a progressive orbital decay toward the centre (orange curve). The right panel shows the corresponding radial evolution as a function of time.

5 Methodology

The present work is based on orbital integration methods using the public code galpy (subsection 5.1).The physical framework of these numerical integrations as the numerical parameters are given in subsection 5.2. To quantify the dynamical friction effect, we need to fix a disruption criterion to compute the fall-in time of the GC into the center of the host galaxy (subsection 5.3).

5.1 Orbital integration with `galpy`

The orbital evolution of globular clusters is computed using the public Python package `galpy` [4]. This code provides a flexible framework for galactic dynamics, allowing orbits to be integrated in a wide range of analytical gravitational potentials. In this work, `galpy` is particularly useful because it allows us to build controlled dark matter halo models and to vary their physical parameters, such as the halo mass, scale radius, and shape.

Our approach is based on test-particle integrations in static analytical potentials. This means that the globular cluster moves in a prescribed gravitational field, while the potential itself does not evolve with time. Such a setup is well suited to our goal, since it allows us to isolate the effect of the dark matter halo geometry on the orbital decay. In particular, we can compare spherical and non-spherical halos while keeping the other parameters fixed.

This method is also computationally efficient. A full N-body treatment would describe the halo and the globular cluster self-consistently, but it would be much more expensive and would make it difficult to explore a large parameter space. By contrast, analytical orbit integrations allow us to test many halo shapes, masses, initial radii, and orbital orientations in a systematic way.

For each model, we first define the gravitational potential of the host dwarf galaxy. We then set the initial position and velocity of the globular cluster and integrate its orbit over the desired timescale. Dynamical friction is included as an additional force term, allowing us to follow the orbital decay.

5.2 Physical framework, parameters, and modelling

In the orbital integrations, the host dwarf galaxy is represented by a dark matter halo only. Although `galpy` allows one to combine several gravitational components, such as a stellar disc, a bulge, a bar, or a dark matter halo, we deliberately neglect the baryonic components in this work. This simplified setup is chosen in order to isolate the role of the dark matter potential in the orbital evolution of globular clusters.

This approximation is motivated by the fact that dwarf galaxies are generally strongly dominated by dark matter. Their stellar and gaseous components are therefore expected to contribute less to the gravitational potential than in more massive galaxies. By neglecting baryons, we avoid introducing additional physical ingredients, such as gas or feedback-driven potential fluctuations, which would make it more difficult to identify the specific impact of the dark matter halo shape on the decay of globular cluster orbits. Moreover, adding baryons would increase the density and therefore strengthen dynamical friction (see Equation 1), making globular clusters fall in even faster. Since the timing problem already arises because the predicted orbital decay is too efficient, neglecting baryons is a conservative choice for the purpose of this study.

The dark matter halo is mainly characterized by its virial mass M_{halo}, its virial radius r_{vir}, and its scale radius r_s. These quantities are related through the concentration parameter

$$c_{\mathrm{vir}} = \frac{r_{\mathrm{vir}}}{r_s}. \tag{6}$$

The virial radius is defined as the radius enclosing a mean density equal to 200 times the critical density of the Universe, while the scale radius sets the characteristic transition scale of the halo density profile. For a given halo mass, the concentration depends on cosmology and redshift. We therefore use the `Colossus` package [6] to assign realistic concentrations to the halos considered in this work. All halo properties are computed at redshift $z = 0$.

The orbiting object is modeled as a globular cluster with fixed properties throughout the analysis. We adopt a mass $M_{\mathrm{obj}} = 10^6\,M_\odot$ and a half-mass radius $r_{\mathrm{hm}} = 10\,\mathrm{pc}$, which are representative values for a typical globular cluster. Because globular clusters are compact compared to the galactic scales considered here, we treat them as point masses when integrating their orbits. This approximation would not be appropriate for extended satellite galaxies, but it is sufficient for the present study, where the internal structure of the cluster is not the main focus.

All orbits are integrated over a time interval of $0 \le t \le 10\,\mathrm{Gyr}$. This timescale is chosen because old globular clusters have ages comparable to a Hubble time. Therefore, whether a cluster can survive for $10\,\mathrm{Gyr}$ without reaching the central region of its host galaxy is directly relevant to the globular cluster timing problem.

5.3 Fall-in criterion

Since dynamical friction causes globular clusters to lose orbital energy and gradually spiral toward the centre of the host galaxy, it is necessary to define a clear criterion to determine when an object can be considered to have fallen in. In this work, the infall time is defined as the first time at which the apocentre of the orbit becomes smaller than $r_{\mathrm{merge}} = 0.2$ kpc, as we already mention in Section 2.

This threshold is motivated by physical considerations. A radius of 200 pc represents a central scale below which a globular cluster can reasonably be considered to have reached the inner region of the galaxy. It is also a characteristic size that can be compared with the extent of nuclear star clusters, which are typically larger than individual globular clusters. Below this radius, the cluster is assumed to have effectively fallen to the centre and to no longer behave as an orbiting outer globular cluster.

6 Theoretical study of globular clusters in dwarf galaxies

We first develop a controlled theoretical framework to isolate the effect of the dark matter halo geometry on the orbital evolution of globular clusters. The goal of this section is to understand how departures from spherical symmetry can modify the efficiency of dynamical friction and, consequently, the time required for a globular cluster to migrate toward the centre of its host galaxy. We therefore consider idealized dark matter potentials, ranging from spherical to flattened configurations, and integrate globular cluster orbits within these potentials. We first describe the adopted elliptical dark matter potential in subsection 6.1, then study how the initial orbital orientation affects the radial decay of the cluster in subsection 6.2 . Finally, we quantify the impact of halo flattening on the infall time and on the critical initial radius from which a globular cluster can reach the central region within a Hubble time (subsection 6.3).

6.1 Elliptical dark matter potential

To model non-spherical dark matter halos, we use the `TwoPowerTriaxialPotential` implemented in `galpy`. This potential is based on a triaxial double power-law density profile of the form

$$\rho(x, y, z) = \frac{\mathrm{M_{halo}}}{A_{NFW} 4\pi r_s^3} \frac{1}{(m/r_s)^{\alpha}\,(1 + m/r_s)^{\beta-\alpha}}, \tag{7}$$

where the ellipsoidal radius m is defined by

$$m^2 = x'^2 + \frac{y'^2}{b^2} + \frac{z'^2}{c^2}. \tag{8}$$

Here, r_s is the scale radius of the halo, while α and β control the inner and outer logarithmic slopes of the density profile, respectively. In particular, the choice $\alpha = 1$ and $\beta = 3$ corresponds to an NFW-like density profile in the spherical limit. The parameters b and c characterize the shape of the halo. When $b = 1$ and $c = 1$, the model reduces to the spherical case, while values different from unity describe departures from spherical symmetry. The primed coordinates (x', y', z') denote the frame aligned with the principal axes of the ellipsoid.

In the present study, we restrict ourselves to the case $c = 1$ and vary only the parameter b. As a result, we do not explore the fully triaxial regime, but only elliptical configurations in the plane. This choice allows us to isolate the effect of in-plane flattening on the orbital evolution of globular clusters while keeping the vertical structure unchanged (see Figure 6).

This class of potentials is particularly well suited to our purpose, since it provides a simple and controlled way to move continuously from a spherical NFW-like halo to an elliptical dark matter halo, and therefore to quantify the impact of halo geometry on dynamical friction and infall times.

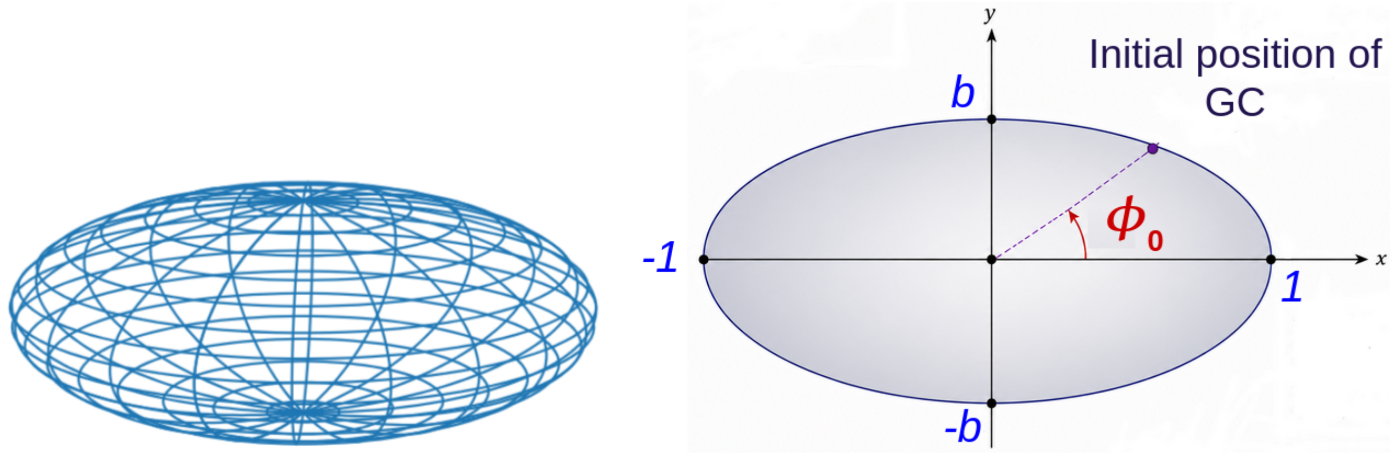

Figure 6: Left panel : Illustration of an ellipsoidal potential. This geometry is characterized by two equal major axes and one shorter minor axis. Right panel : Schematic representation of the initial position of a globular cluster inside a flattened potential. The orbit starts at an angle ϕ_0 with respect to the major axis of the ellipse. The parameter b controls the flattening of the potential, with $b < 1$ corresponding to compression along the y direction. If $b = 1$, it is a NFW spherical potential.

6.2 Influence of halo geometry on the dynamics of globular clusters

We now investigate how the geometry of the dark matter halo affects the orbital evolution of a globular cluster. The cluster is modeled with a mass and a half-mass radius

$$M_{\rm GC} = 10^6\, M_\odot, \qquad r_{\rm hm,GC} = 10\,{\rm pc}.$$

It is initially placed at a galactocentric distance $R_0 = 2\,{\rm kpc}$ in the plane of the galaxy, with $z_0 = 0, v_{z,0} = 0$. The host dwarf galaxy is described by a dark matter halo of mass

$$M_{\rm halo} = 10^9\, M_\odot,$$

with scale radius $r_s = 1.36\,{\rm kpc}$ and virial radius $r_{\rm vir} = 25.66\,{\rm kpc}$. The dark matter halo is represented by a double power-law potential with

$$\alpha = 1, \qquad \beta = 3,$$

corresponding to an NFW-like profile in the spherical limit (see Section 6.1). Two geometries are compared: a spherical halo, defined by $(b = 1, c = 1)$ and an elliptical halo, defined by $(b = 0.6, c = 1)$. In the latter case, the halo is flattened in the plane while the vertical structure is kept unchanged.

The initial orbit is chosen to be nearly circular. The tangential velocity is fixed using the circular velocity of the spherical model at R_0,

$$v_{T,0} = v_{\rm circ,sph}(R_0)\sqrt{1+e},$$

with $e = 0$. This gives an initial velocity of the order of $v_{T,0} \sim 20\,{\rm km\,s^{-1}}$. For a spherical potential, the circular velocity is defined by

$$v^2_{\rm circ,sph}(R) = R\, \left.\frac{\partial \Phi_{\rm sph}}{\partial R}\right|_R,$$

or equivalently,

$$v_{\rm circ,sph}(R) = \sqrt{\frac{GM(<R)}{R}},$$

where $M(< R)$ is the mass enclosed within radius R. The same initial velocity is used in both the spherical and elliptical cases, allowing us to isolate the effect of the halo geometry on the orbital decay. This choice is also motivated by the observational context. For observed globular clusters, for instance in samples identified with surveys such as *Euclid*, we generally have access to their projected positions, but not to their full three-dimensional velocities. Assigning the same circular velocity to the clusters therefore provides a simple and reproducible prescription for initializing the orbits, while allowing us to focus on the effect of the dark matter halo geometry rather than on uncertain velocity initial conditions.

To explore the role of the initial orbital orientation, we consider three initial azimuthal angles (see the right panel of Figure 6),

$$\phi_0 = 0, \qquad \phi_0 = \frac{\pi}{4}, \qquad \phi_0 = \frac{\pi}{2}.$$

For each configuration, the orbit is integrated over 10 Gyr. Dynamical friction is included through the Chandrasekhar prescription, allowing us to follow the progressive loss of orbital energy and angular momentum of the globular cluster (see Figure 7).

The first effect comes from the flattening of the dark matter potential itself. In an elliptical halo, the gravitational field is no longer identical in all directions, and the orbit of the globular cluster differs from the spherical reference case. The cluster can reach larger apocentric distances and spend more time in the outer regions of the halo. Since dynamical friction depends on the local background density, it becomes weaker in these less dense regions. As a result, the loss of orbital energy and angular momentum is less efficient, and the infall of the cluster is delayed.

The second effect comes from the initial angular position of the globular cluster, described by ϕ_0. Different values of ϕ_0 make the cluster sample different directions of the elliptical potential. This is particularly visible for $\phi_0 = \frac{\pi}{2}$, shown by the green curve. In this case, the cluster initially moves along the flattened direction of the potential, which leads to a more eccentric orbit and a larger apocentre. The cluster therefore spends an even larger fraction of its time in the outer, low-density regions, where dynamical friction is weaker.

This demonstrates that the orbital decay of globular clusters is affected both by the global shape of the dark matter halo and by the initial orientation of the orbit. Even at fixed halo mass, initial radius, and cluster mass, changing the halo geometry or the initial angle ϕ_0 can significantly modify the infall time.

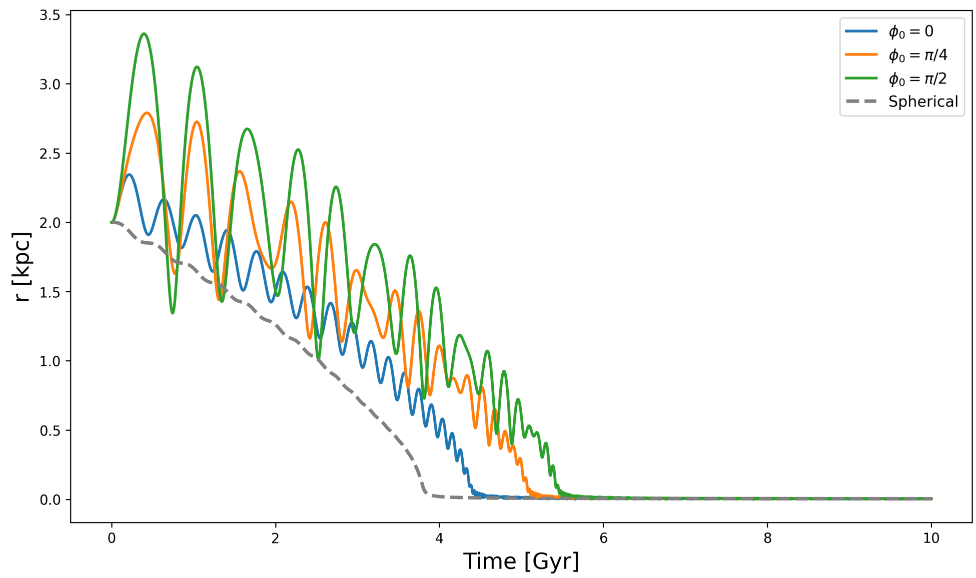

Figure 7: Radial evolution of a GC orbit in an elliptical dark matter potential for different initial angular positions ϕ_0. The curves show the 3D distance r from the galaxy centre as a function of time. The dashed grey curve corresponds to the spherical reference case, while the coloured curves correspond to elliptical configurations ($b = 0.6, c = 1$) with $\phi_0 = 0$, $\pi/4$, and $\pi/2$.

6.3 Fall-in of globular clusters

The previous results show that the orbital decay of a globular cluster depends on both the geometry of the host dark matter halo and the initial orbital orientation. We now quantify this effect by defining an infall time, $t_{\rm fall}$, as the time at which the first apocentre of the orbit falls below a threshold radius $r_{\rm merge} = 0.2$ kpc (see Section 5.3). This radius is used as a criterion to determine whether the globular cluster has reached the central region of the dwarf galaxy.

We first compute a reference infall time in the spherical halo, denoted $t_{\rm fall,sph}$, corresponding to the case $b = 1$ and $c = 1$. For the reference model considered here, this spherical infall time is approximately $t_{\rm fall,sph} \simeq 4\,{\rm Gyr}$ (see Figure 7) We then repeat the calculation for a grid of elliptical halos, varying the flattening parameter b from 0.1 to 1.0, while keeping $c = 1$. For each value of b, we also vary the initial azimuthal angle ϕ_0 between $0°$ and $90°$. By symmetry, this angular range is sufficient to capture all distinct orbital configurations in the flattened potential. The globular cluster is initially placed at $R_0 = 2\,{\rm kpc}$. For all models, the initial tangential velocity is fixed to the circular velocity of the spherical halo, as discussed in Section 6.2.

Figure 8 shows the ratio

$$\frac{t_{\rm fall}}{t_{\rm fall,sph}}$$

as a function of the initial angle ϕ_0 and the flattening parameter b. Values larger than unity indicate that the elliptical halo delays the infall compared to the spherical case.

The figure shows that the infall time is strongly affected by the flattening of the potential. For nearly spherical halos, $b \simeq 1$, the ratio remains close to unity for all initial angles, meaning that the orbital decay is similar to the spherical reference case. As b decreases, the infall time increases significantly. For $b \sim 0.6$, the infall time is already about 1.5 times larger than in the spherical case, while for $b \sim 0.3$ it can reach values above 2. This indicates that a strongly flattened potential can substantially slow down the inward migration of the cluster.

The dependence on the initial angle ϕ_0 is weaker than the dependence on the flattening parameter b, but it remains visible. At fixed b, orbits starting closer to $\phi_0 = \pi/2$ generally fall in more slowly, as already seen in Section 6.2. The dominant effect in this regime is therefore the flattening of the halo itself rather than the precise initial angular position.

The white regions correspond to configurations where the GC does not fall into the center of the galaxy. In practice, this occurs for the most flattened halos, where the orbital decay becomes so inefficient that the cluster does not reach the central region within the integration time (10 Gyr).

Overall, this analysis shows that the geometry of the dark matter halo can strongly modify the efficiency of dynamical friction. A flattened halo generally increases the infall time of globular clusters, and in the most extreme cases can prevent their migration to the central region altogether.

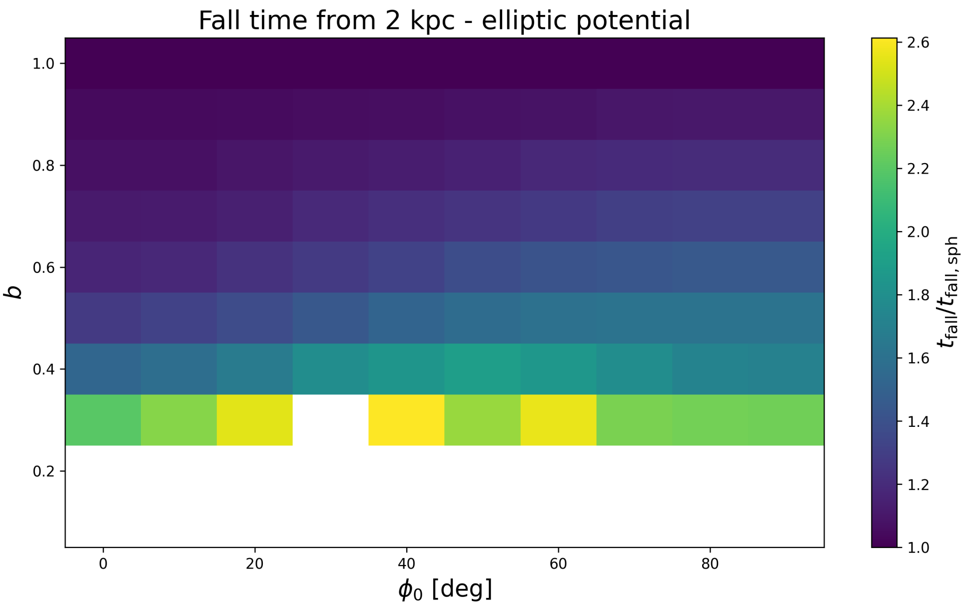

Figure 8: Ratio of the globular cluster infall time in an elliptical dark matter potential to the infall time in the corresponding spherical potential. The cluster is initially placed at $r_0 = 2\,{\rm kpc}$. The horizontal axis shows the initial angular position ϕ_0, while the vertical axis shows the axis ratio b, which controls the flattening of the potential. The color scale gives $t_{\rm fall}/t_{\rm fall,sph}$. Values larger than unity indicate that the elliptical potential increases the infall time compared to the spherical case, while values close to unity correspond to a similar decay time. White regions correspond to configurations where the GC does not fall into the center of the galaxy.

To make the analysis more robust, we then remove the assumption of a fixed initial position for the globular cluster. Instead, for each halo model, we determine the critical initial radius from which the cluster is able to reach the central region of the dwarf galaxy within 10 Gyr. This timescale is physically motivated, as it is comparable to the typical age of old globular cluster systems and therefore provides a useful criterion for assessing whether a cluster could have survived until the present day. For a given value of the flattening parameter b, the critical radius $r_{init,\mathrm{crit}}$ is therefore defined by

$$t_{\mathrm{fall}}(r_{init,\mathrm{crit}}) = 10\,\mathrm{Gyr}.$$

To determine this radius, we first explore a grid of approximately 40 initial radii r_{init} in order to bracket the solution, such that $t_{\mathrm{fall}}(r_{init,\mathrm{min}}) < 10\,\mathrm{Gyr}$, and $t_{\mathrm{fall}}(r_{init,\mathrm{max}}) > 10\,\mathrm{Gyr}$. A bisection method is then applied between these two radii until the infall time satisfies $9.99\,\mathrm{Gyr} < t_{\mathrm{fall}}(r_{init,\mathrm{crit}}) < 10.01\,\mathrm{Gyr}$. corresponding to a 1% tolerance around 10 Gyr. This procedure gives, for each halo shape, the maximum initial radius from which a globular cluster can fall to the centre within 10 Gyr.

Figure 9 shows the results for $M_{\mathrm{halo}} = 10^9\,M_\odot$. We sample 35 values of the flattening parameter b, with a denser sampling toward small b, where the variation of the critical radius is strongest. The calculation is repeated for three initial azimuthal angles,

$$\phi_0 = 0, \qquad \phi_0 = \frac{\pi}{4}, \qquad \phi_0 = \frac{\pi}{2}.$$

The critical radius is small for low values of b. This is consistent with the previous result: when the halo is strongly flattened, the infall time is increased, and the globular cluster must therefore start from a smaller radius in order to reach the central region within 10 Gyr. As the halo becomes more spherical, with $b \to 1$, the critical radius approaches the spherical reference value.

The initial azimuthal angle also affects the orbital decay. In general, the case $\phi_0 = \pi/2$ leads to a slower infall, as already seen in Figures 7 and 8, because the cluster samples the flattened direction of the potential more strongly. However, the difference between the different initial angles becomes much less visible for strongly flattened halos, especially below $b \simeq 0.4$, where the curves nearly converge.

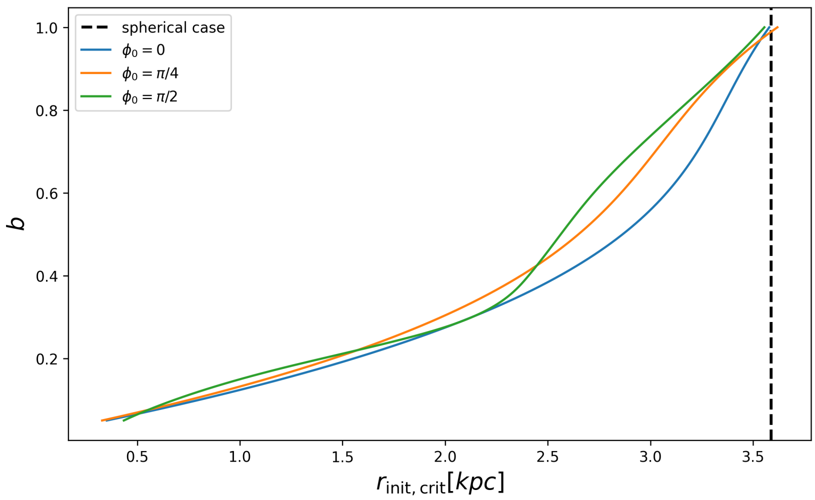

Figure 9: Critical initial radius for the infall of a globular cluster within 10 Gyr, shown as a function of the halo flattening parameter b. For each value of b, $r_{\mathrm{init,crit}}$ is the maximum initial radius from which the cluster reaches the central region within 10 Gyr. It shows the smoothed results for three initial azimuthal angles, $\phi_0 = 0$, $\pi/4$, and $\pi/2$. The vertical dashed line indicates the spherical case, $b = 1$.

We finally repeat the calculation for three different halo masses, fixing the initial azimuthal angle to $\phi_0 = 0$. This choice corresponds to the most conservative case for the timing problem: among the initial orientations considered, $\phi_0 = 0$ generally leads to the fastest infall. Therefore, if a globular cluster is not able to reach the central region within 10 Gyr in this configuration, it is unlikely to do so for less favourable initial orientations. The results are shown in Figure 10. The critical radius depends strongly on the halo mass. In our setup, increasing the halo mass also changes the scale radius of the halo. The more massive halos are therefore more extended and less dense. As a result, dynamical friction becomes less efficient, the globular cluster decays more slowly, and the critical initial radius becomes smaller. In other words, for a globular cluster to reach the centre within 10 Gyr, it must start closer to the centre in the most massive halo models.

The case $M_{\rm halo} = 10^{11}\,M_\odot$ is particularly interesting. For this model, the behaviour at $b \gtrsim 0.5$ does not follow the simple trend found at lower masses, where the critical radius generally decreases as b increases. However, this result should be interpreted with caution, since $10^{11}\,M_\odot$ is close to the upper mass limit expected for dwarf galaxy halos. This regime is therefore a limiting case.

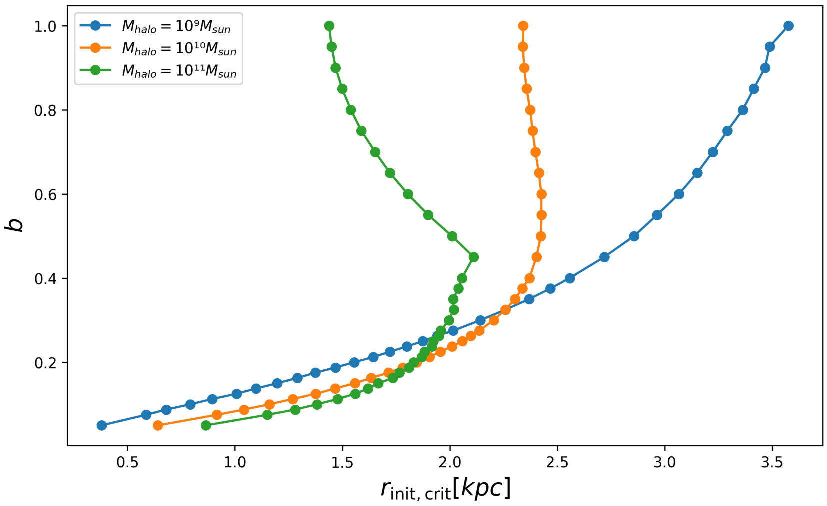

Figure 10: Critical initial radius for the infall of a globular cluster within 10 Gyr, shown as a function of the halo flattening parameter b for three different dark matter halo masses. The initial angle is fixed to $\phi_0 = 0$.

As an additional check, we also explored a fully triaxial configuration by varying the vertical axis ratio c, while keeping the same procedure used to compute the critical initial radius. Figure 15 shows $r_{\rm init,crit}$ as a function of the in-plane flattening parameter b, for several values of c. The case $c = 1$ corresponds to the two-dimensional flattened models studied above, while smaller values of c introduce an additional flattening along the vertical direction.

The curves remain relatively close to each other over most of the parameter range, indicating that changing c does not strongly modify the critical radius compared to the dominant effect of varying b. In other words, the infall time is mainly controlled by the in-plane flattening explored in the previous sections, while the additional triaxial deformation produces only secondary changes. This suggests that the two-dimensional study with $c = 1$ captures the main effect of halo geometry on the orbital decay, and is therefore a relevant approximation for the purpose of this work.

7 Comparison with the literature

The previous sections showed that the geometry of the dark matter halo can significantly affect the orbital decay of globular clusters. In order to check that our numerical framework gives physically reasonable results, we now compare it with an existing study of orbital decay in non-spherical halos. We use the work of Peñarrubia et al.(2004) [13] as a reference, since they studied the evolution of a satellite galaxy in a non-spherical dark matter potential.

Peñarrubia et al. (2004) considered a host galaxy with mass $M_h = 7.84 \times 10^{11}\,M_\odot$ and a satellite galaxy with mass $M_s = 5.60 \times 10^9\,M_\odot$. Their host halo is described by a non-spherical isothermal dark matter potential. Although our model is based on a double-power-law triaxial halo rather than on the exact potential used in their work, we choose parameters that allow us to reproduce as closely as possible the density profile and orbital behaviour of their reference model.

Figure 14 compares the density profiles along the three principal axes x, y, and z. The blue curves correspond to the model of Peñarrubia et al. (2004), while the orange dashed curves show our elliptical double-power-law halo model. The parameters of our model, in particular r_s, α, and β, were chosen so as to reproduce the overall radial behaviour of the Peñarrubia et al. density profile along the different axes. The agreement is good over most of the radial range, showing that our analytical halo provides a reasonable approximation to the reference model.

We then use the same satellite mass and choose a half-mass radius close to the characteristic size of their satellite model. This comparison should therefore be understood as a consistency check rather than a one-to-one reproduction. Since the two models do not use the same analytical potential and since Peñarrubia et al. rely on N-body simulations, the objective is to recover the same qualitative behaviour of the orbital decay rather than an exact match at all radii and times.

The parameters used in Peñarrubia et al.(2004) and in our corresponding model are summarized in Tables 1 and 2. To compare with their Fig. 3a, we adopt an eccentric orbit with $e = 0.5$ and an initial angle $\phi_0 = 0$. The initial tangential velocity is set to $v_{T,0} = 100\,\mathrm{km\,s^{-1}}$, which allows us to recover approximately the eccentricity used in their study. A key difference between the two approaches is the treatment of dynamical friction. In Peñarrubia et al. (2004), the decay is produced self-consistently by the N-body interaction between the satellite and the live halo. In our case, the background halo is fixed and analytical, and dynamical friction is added explicitly through a Chandrasekhar-like force.

Table 1: Comparison between the dark matter halo parameters adopted adopted by Peñarrubia et al. (2004) [13] and those used in this work. In the Peñarrubia et al. model, q_h denotes the axis ratio of the non-spherical halo and γ is the core radius. Our model uses a double-power-law triaxial halo. The parameters b and c define the axis ratios of the potential, while α and β set the inner and outer slopes of the profile.

DM Halo	**Symbol**	**Value**
Peñarrubia 04	M_h	$7.84 \times 10^{11}\ M_\odot$
	q_h	0.60
	γ	3.5 kpc
Our study	M_{halo}	$7.84 \times 10^{11}\ M_\odot$
	r_s	7.70 kpc
	b	0.6
	c	1.0
	α	0.0
	β	3.0

Table 2: Satellite parameters adopted in Peñarrubia et al. (2004) and in this work. The Peñarrubia et al. model describes the satellite using a total mass M_s, a core radius r_c, a tidal radius r_t, and a mean radius $\langle r\rangle$. In this work, the satellite is modeled with the same total mass and characterized by its half-mass radius r_{hm}.

Satellite	**Symbol**	**Value**
Peñarrubia 04	M_s	$5.60 \times 10^{9}\ M_\odot$
	r_c	0.67 kpc
	r_t	7.24 kpc
	$\langle r\rangle$	1.64 kpc
Our study	M_s	$5.60 \times 10^{9}\ M_\odot$
	r_{hm}	1.5 kpc

The three panels shown in Figure 11 correspond respectively to the initial angles $\phi_0 = 0$, $\phi_0 = \pi/4$, and $\phi_0 = \pi/2$. The white points are the reference results from the N-body simulations of Peñarrubia et al.(2004). For the comparison, the total integration time is chosen such that the final time of each orbit corresponds to the time of the last white point in the corresponding Peñarrubia et al. simulation. The aim is therefore not to reproduce every point exactly, but to recover the overall orbital decay trend.

The blue curves show our ellipsoidal model, while the orange curves correspond to the spherical version of the same model. The comparison shows that the global behaviour of the N-body results is reasonably well reproduced, and that the ellipsoidal model better captures the effect of halo non-sphericity on the orbital decay : we recover the trend that increasing the initial angle ϕ_0 slows down the orbital decay. In particular, the $\phi_0 = \pi/2$ case shows a less rapid decline than the $\phi_0 = 0$ case, consistent with the behaviour found in Peñarrubia et al.(2004). Nevertheless, our model appears to predict orbital decay that is still too efficient compared to the reference simulation. For example, in the case $\phi_0 = \pi/2$, Peñarrubia et al. (2004) find an infall time of about 6.5 Gyr, whereas our model predicts an infall time of approximately 5 Gyr.

This discrepancy is consistent with the conclusions of Peñarrubia et al. (2004). In their study, they tested different analytical descriptions of dynamical friction in order to reproduce their N-body simulations. They found that the classical Chandrasekhar formula was not sufficient to fully explain the orbital decay. Instead, they showed that a better agreement could be obtained by accounting for an anisotropic velocity dispersion field (Binney 1977 [2]), which modifies both the amplitude and the direction of the dynamical friction force.

This suggests that the remaining differences in our comparison may come from the simplified form of the dynamical friction prescription used in this work. For this reason, I am currently investigating the implementation of an anisotropic dynamical friction model, following this more general approach.

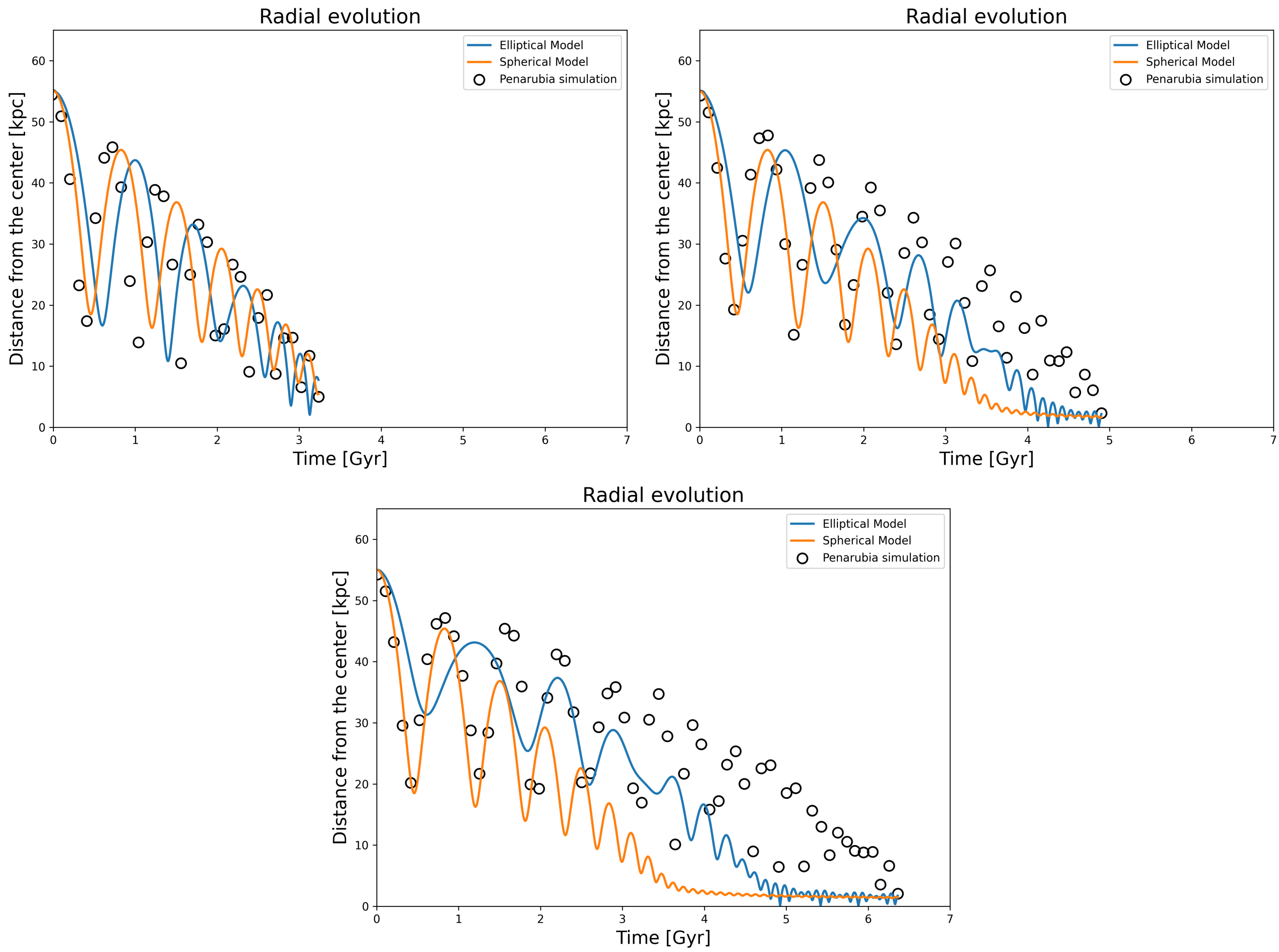

Figure 11: Comparison with the orbital decay results of Peñarrubia et al. (2004) [13] for three different initial angular positions: $\phi_0 = 0$, $\phi_0 = \pi/4$, and $\phi_0 = \pi/2$. The white points correspond to the simulation data from Peñarrubia et al. and are used as the reference to be reproduced. The maximum integration time shown in each panel is chosen to match the position of the last white point. The blue curves show our ellipsoidal model, while the orange curves show the corresponding spherical model.

8 Conclusion and perspectives

In this report, we investigated whether the shape of the dark matter potential in dwarf galaxies can affect the orbital decay of globular clusters and therefore help understand the globular cluster timing problem. This problem arises because, in dense CDM halos, dynamical friction can be efficient enough to make globular clusters spiral toward the galaxy centre within a few Gyr, whereas several systems are still observed at large galactocentric radii.

We first developed a controlled theoretical framework based on orbit integrations in analytical dark matter potentials. Using `galpy`, we compared spherical and flattened NFW-like halos, while keeping the globular cluster mass, size, and initial conditions fixed. The results show that halo geometry has a significant impact on the orbital decay. In particular, flattened potentials can increase the infall time compared to the spherical case. The effect also depends on the initial angular position of the cluster: orbits starting closer to the flattened direction generally decay more slowly. This confirms that the infall time is not determined only by the halo mass and initial radius, but also by the geometry of the gravitational potential.

We then quantified this effect by computing the ratio

$$\frac{t_{\mathrm{fall}}}{t_{\mathrm{fall,sph}}},$$

where $t_{\mathrm{fall,sph}}$ is the infall time in the corresponding spherical halo. For strongly flattened halos, the infall time can be increased by factors of order 2 or more, and in some cases the globular cluster does not reach the central region within the integration time. We also introduced a critical initial radius $r_{\mathrm{init,crit}}$, defined as the maximum initial radius from which a globular cluster can reach the central region within 10 Gyr. This provides a useful way to connect the model to the survival of old globular cluster systems.

To check that our approach gives physically reasonable results, we compared our model with the N-body study of Peñarrubia et al. (2004) [13]. We recover the same qualitative behaviour. In particular, the orbital decay becomes slower when the initial angle is increased, with the $\phi_0 = \pi/2$ case decaying less rapidly than the $\phi_0 = 0$ case. This comparison supports the validity of our framework for studying the qualitative impact of non-spherical halo shapes.

Finally, we used the `TNG50` cosmological simulation to estimate the typical shapes of dark matter halos associated with dwarf galaxies. We first validated the shape-measurement pipeline on artificial NFW halos and showed that at least $N_{\mathrm{DM}} \gtrsim 1000$ particles are needed to obtain reliable global axis ratios. Applying this criterion to the TNG50 dwarf galaxy sample, we found that the dark matter halos are generally non-spherical, with typical global axis ratios around

$$b \sim 0.75, \qquad c \sim 0.85,$$

and with substantial halo-to-halo scatter. This result provides a cosmological motivation for exploring non-spherical potentials.

Several limitations remain. First, the orbital integrations were performed in static analytical potentials, whereas real dwarf galaxies evolve with time and may experience tidal interactions with their environment. This could be improved by using cosmological simulations to follow the evolution of the host potential across snapshots, measuring quantities such as the halo mass, scale radius, concentration, and shape as a function of time. The globular cluster orbits could then be integrated in a time-dependent potential, providing a more realistic description of their long-term evolution. Second, the dynamical friction force was modeled using a Chandrasekhar like prescription, which assumes an idealized background velocity distribution. In non-spherical systems, the velocity dispersion tensor can be anisotropic, and this may modify the direction and amplitude of the friction force. Third, baryonic components, and globular cluster mass loss were neglected, although these effects may also influence the survival of globular clusters.

Future work should therefore extend the present study in several directions. A first improvement, which I am currently working on, is to implement in `galpy` a more general dynamical friction prescription adapted to anisotropic velocity distributions. This implementation is based on the formalism introduced by Binney (1977) [2], in which the background velocity dispersion is anisotropic rather than by a single isotropic Maxwellian dispersion. Such a prescription would be more appropriate for non-spherical dark matter halos and would allow the dynamical friction force to be treated more consistently in flattened or triaxial potentials.

In parallel, I am also currently investigating observational data from *Euclid*, in particular the distances and masses of globular clusters in dwarf galaxies. This will allow us to test more directly how the flattening of the dark matter potential may affect the orbital decay of observed globular cluster systems, and whether non-spherical halo geometries can help explain their present-day positions.

Another interesting perspective would be to extend this analysis to alternative dark matter models, such as fuzzy dark matter. Unlike the cuspy CDM-like density profiles used in this report, fuzzy dark matter models can produce cored central density profiles. This reduction of the central dark matter density could weaken dynamical friction and therefore slow down the orbital decay of globular clusters, as suggested by Dome et al. (2022) [7].

Overall, this work shows that the shape of the dark matter potential is an important ingredient in the orbital evolution of globular clusters. Non-spherical halos can delay orbital decay and increase globular cluster survival times, suggesting that halo geometry may contribute to resolving, or at least weakening, the globular cluster timing problem in dwarf galaxies.

9 Bibliography

References

[1] N. and Aghanim et al. “¡i¿Planck¡/i¿ 2018 results: VI. Cosmological parameters”. In: *Astronomy amp; Astrophysics* 641 (2020), A6. ISSN: 1432-0746. DOI: `10.1051/0004-6361/201833910`. URL: `http://dx.doi.org/10.1051/0004-6361/201833910`.

[2] J. Binney. “Dynamical friction in aspherical clusters.” In: 181 (Dec. 1977), pp. 735–746. DOI: `10.1093/mnras/181.4.735`.

[3] Pierre Boldrini, Roya Mohayaee, and Joseph Silk. “Embedding globular clusters in dark matter minihaloes solves the cusp–core and timing problems in the Fornax dwarf galaxy”. In: *Monthly Notices of the Royal Astronomical Society* 492.3 (Jan. 2020), pp. 3169–3178. ISSN: 1365-2966. DOI: `10.1093/mnras/staa011`. URL: `http://dx.doi.org/10.1093/mnras/staa011`.

[4] Jo Bovy. “galpy: A python LIBRARY FOR GALACTIC DYNAMICS”. In: *The Astrophysical Journal Supplement Series* 216.2 (Feb. 2015), p. 29. ISSN: 1538-4365. DOI: `10.1088/0067-0049/216/2/29`. URL: `http://dx.doi.org/10.1088/0067-0049/216/2/29`.

[5] S. Chandrasekhar. “Dynamical Friction. I. General Considerations: the Coefficient of Dynamical Friction.” In: 97 (Mar. 1943), p. 255. DOI: `10.1086/144517`.

[6] Benedikt Diemer. “COLOSSUS: A Python Toolkit for Cosmology, Large-scale Structure, and Dark Matter Halos”. In: *The Astrophysical Journal Supplement Series* 239.2 (Dec. 2018), p. 35. ISSN: 1538-4365. DOI: `10.3847/1538-4365/aaee8c`. URL: `http://dx.doi.org/10.3847/1538-4365/aaee8c`.

[7] Tibor Dome et al. “On the cosmic web elongation in fuzzy dark matter cosmologies: Effects on density profiles, shapes, and alignments of haloes”. In: *Monthly Notices of the Royal Astronomical Society* 519.3 (Dec. 2022), pp. 4183–4202. ISSN: 1365-2966. DOI: `10.1093/mnras/stac3766`. URL: `http://dx.doi.org/10.1093/mnras/stac3766`.

[8] Rain Kipper et al. “Tidal forces from the wake of dynamical friction: warps, lopsidedness, and kinematic misalignment”. In: 498.1 (Oct. 2020), pp. 1080–1092. DOI: `10.1093/mnras/staa2486`. arXiv: `2008.07177 [astro-ph.GA]`.

[9] Gigi Y C Leung et al. “A dwarf–dwarf merger and dark matter core as a solution to the globular cluster problems in the Fornax dSph”. In: *Monthly Notices of the Royal Astronomical Society* 493.1 (Dec. 2019), pp. 320–336. ISSN: 1365-2966. DOI: `10.1093/mnras/stz3017`. URL: `http://dx.doi.org/10.1093/mnras/stz3017`.

[10] Noah Meadows et al. “Cusp or core? Revisiting the globular cluster timing problem in Fornax”. In: 491.3 (Jan. 2020), pp. 3336–3342. DOI: `10.1093/mnras/stz3280`. arXiv: `1910.11887 [astro-ph.GA]`.

[11] Julio F. Navarro, Carlos S. Frenk, and Simon D. M. White. “A Universal Density Profile from Hierarchical Clustering”. In: *The Astrophysical Journal* 490.2 (Dec. 1997), pp. 493–508. ISSN: 1538-4357. DOI: `10.1086/304888`. URL: `http://dx.doi.org/10.1086/304888`.

[12] Se-Heon Oh et al. “THE CENTRAL SLOPE OF DARK MATTER CORES IN DWARF GALAXIES: SIMULATIONS VERSUS THINGS”. In: *The Astronomical Journal* 142.1 (2011), p. 24. ISSN: 1538-3881. DOI: `10.1088/0004-6256/142/1/24`. URL: `http://dx.doi.org/10.1088/0004-6256/142/1/24`.

[13] Jorge Peñarrubia, Andreas Just, and Pavel Kroupa. “Dynamical friction in flattened systems: a numerical test of Binney’s approach”. In: *Monthly Notices of the Royal Astronomical Society* 349.2 (Apr. 2004), pp. 747–756. ISSN: 1365-2966. DOI: `10.1111/j.1365-2966.2004.07549.x`. URL: `http://dx.doi.org/10.1111/j.1365-2966.2004.07549.x`.

10 Appendix

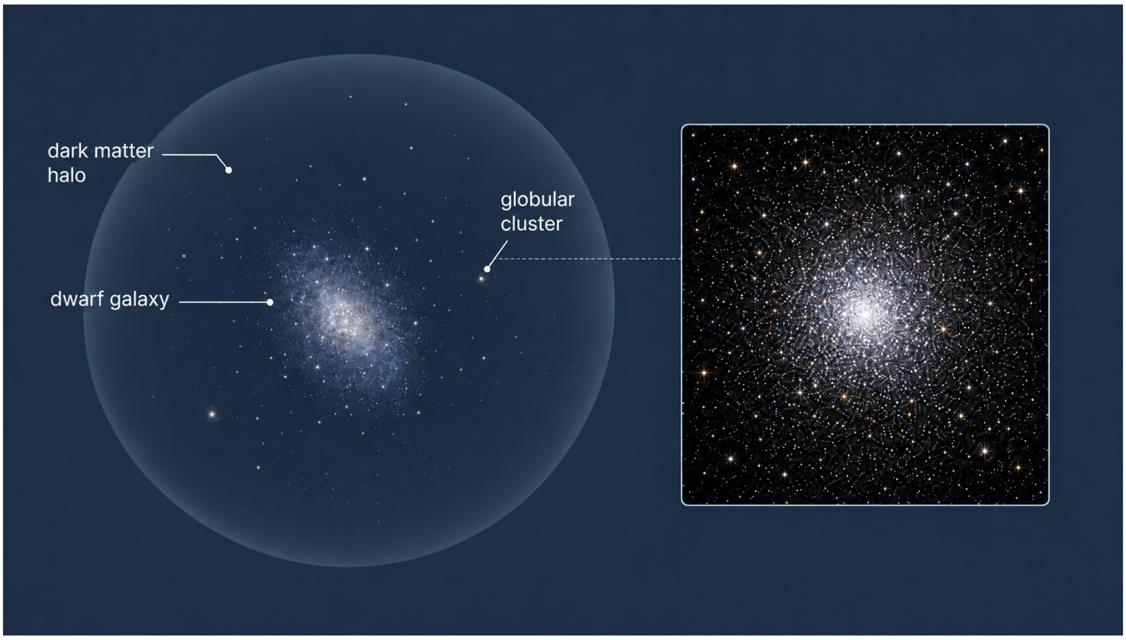

Figure 12: Schematic illustration of a dwarf galaxy embedded in its extended dark matter halo, together with an orbiting globular cluster. The right panel shows an observed globular cluster, used here as an illustrative example of the type of stellar system whose orbital decay is studied. Image credit: The Hubble Heritage Team (AURA/STScI/NASA/ESA).

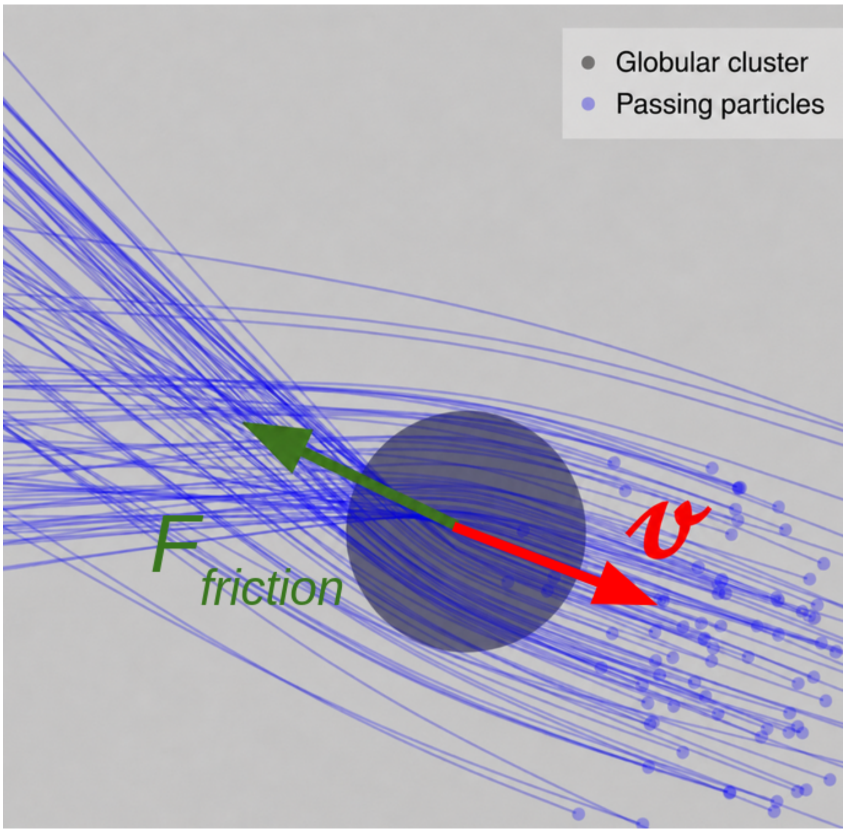

Figure 13: Illustration of the density wake's production. The trajectory of a sample of Dark Matter particles is shown in blue, the red arrow indicates the direction of motion of the galaxy. The green arrow indicates the direction of the dynamical friction force opposite to the cluster motion. Figure taken from Kipper et al. 2020 [8]

.

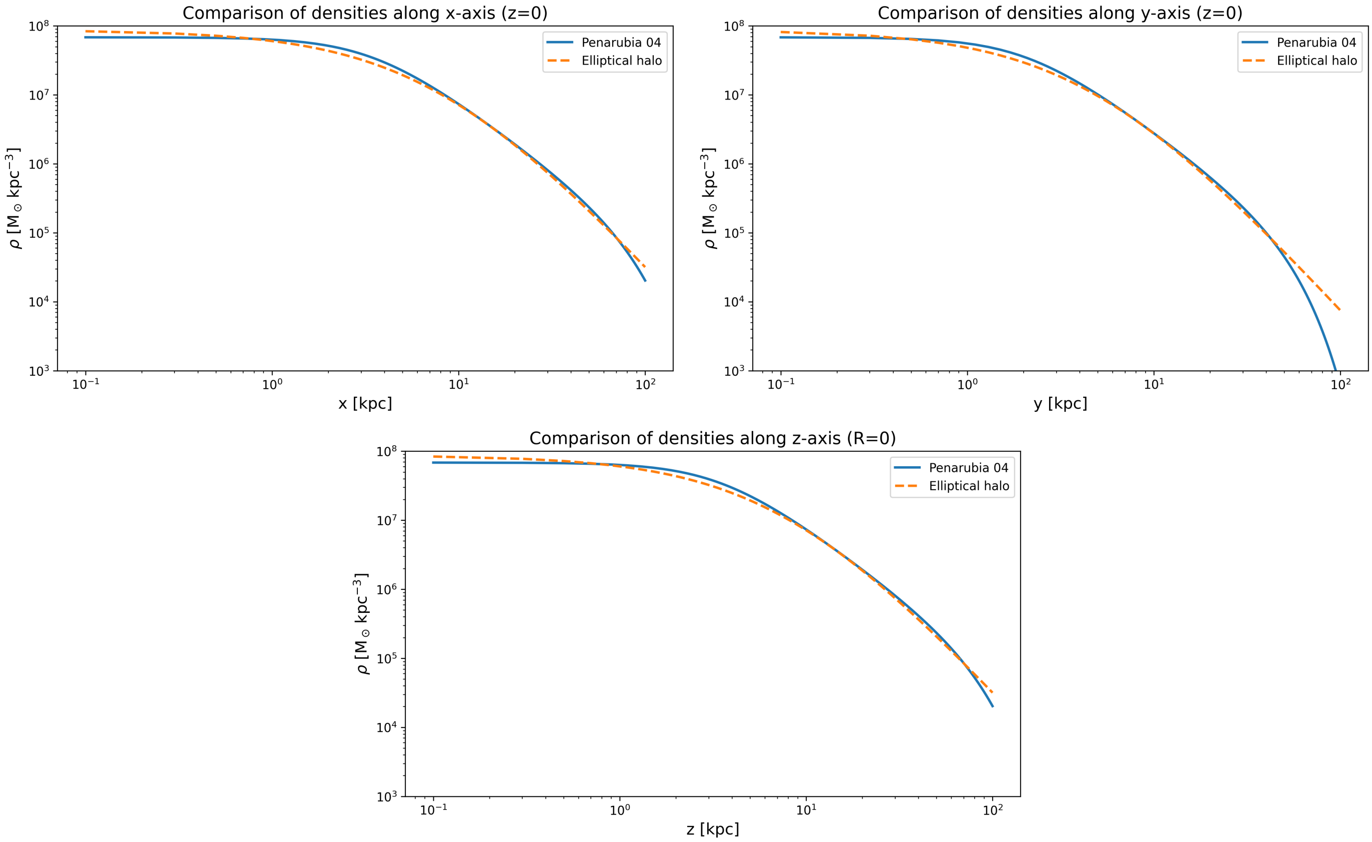

Figure 14: Comparison of the dark matter density profiles along the three principal axes. The solid blue curves show the density profile adopted by Peñarrubia et al. (2004) [13], while the dashed orange curves correspond to the elliptical halo model used in this work. The parameters of our model, in particular the inner slope α, the outer slope β, and the scale radius r_s, were adjusted in order to reproduce the overall radial behaviour of the reference profiles along the three axes.

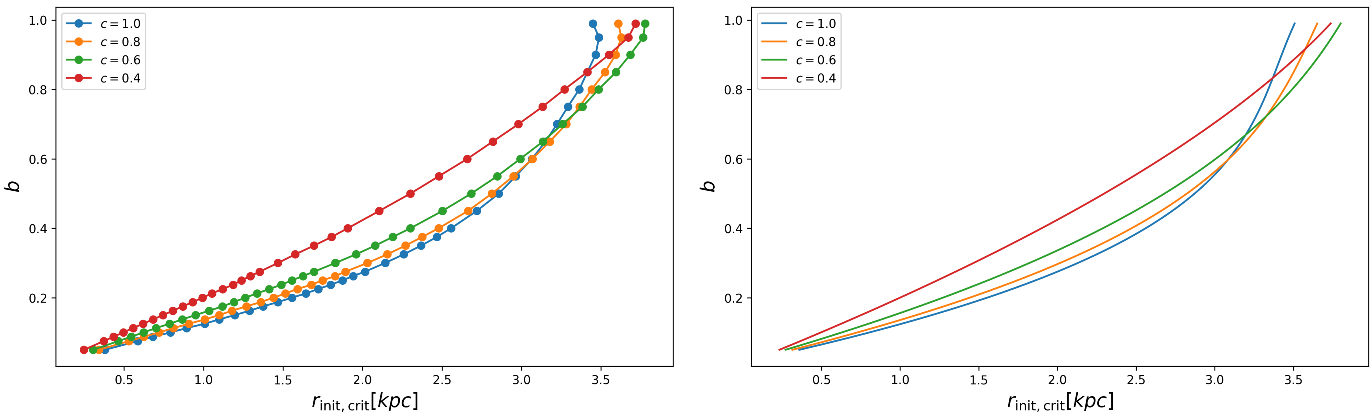

Figure 15: Left panel : Critical initial radius for the infall of a globular cluster within 10 Gyr, shown as a function of the in-plane flattening parameter b for different values of the vertical axis ratio c. The case $c = 1$ corresponds to the flattened two-dimensional models used in the main analysis, while lower values of c represent more triaxial configurations. The right panel shows the same results smoothed with a `UnivariateSpline` interpolator with smoothing parameter $s = 0.01$

Table 3: Best-fitting parameters for the relation between the global dark matter halo axis ratios and dark matter mass in the TNG50 dwarf galaxy sample. The fitted relation is $y = C_1 + C_2[\log_{10}(M_{\rm DM}/M_\odot) - 10]$, where y is either b or c.

Axis ratio	**Intercept** C_1	**Slope** C_2
b	0.743	-0.037
c	0.820	-0.023

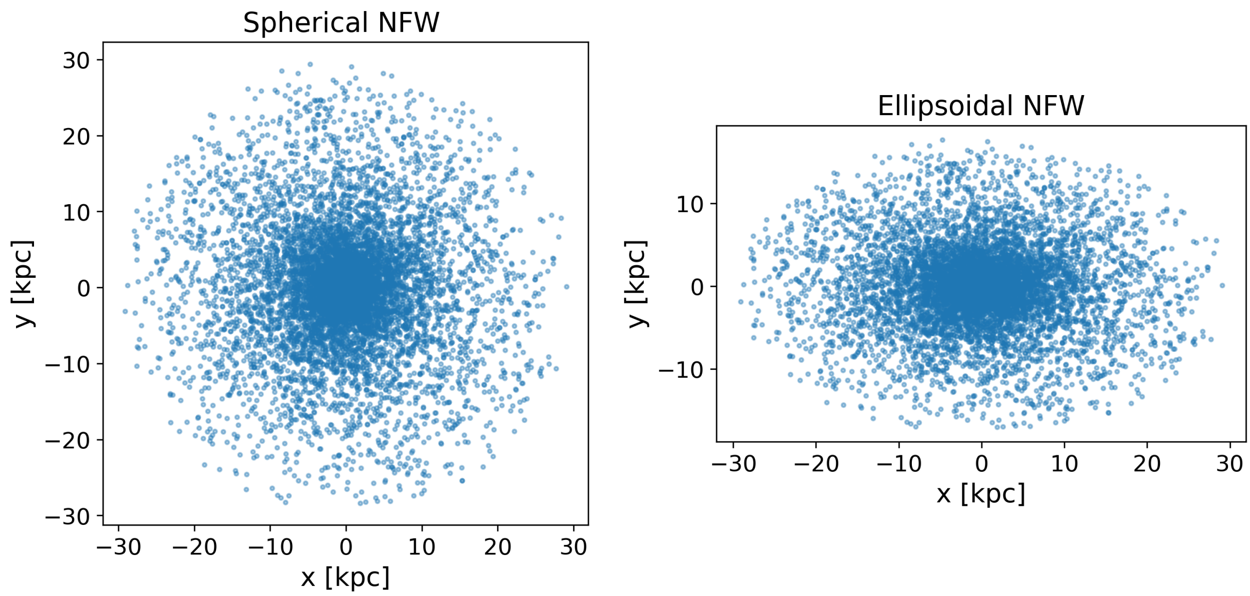

Figure 16: Projected particle distributions for the artificial NFW halos used to validate the shape-measurement pipeline. The left panel shows a spherical NFW halo and the right panel shows an ellipsoidal NFW halo ($b = 0.6, c = 1.0.$) obtained by rescaling the spherical distribution along one axis.

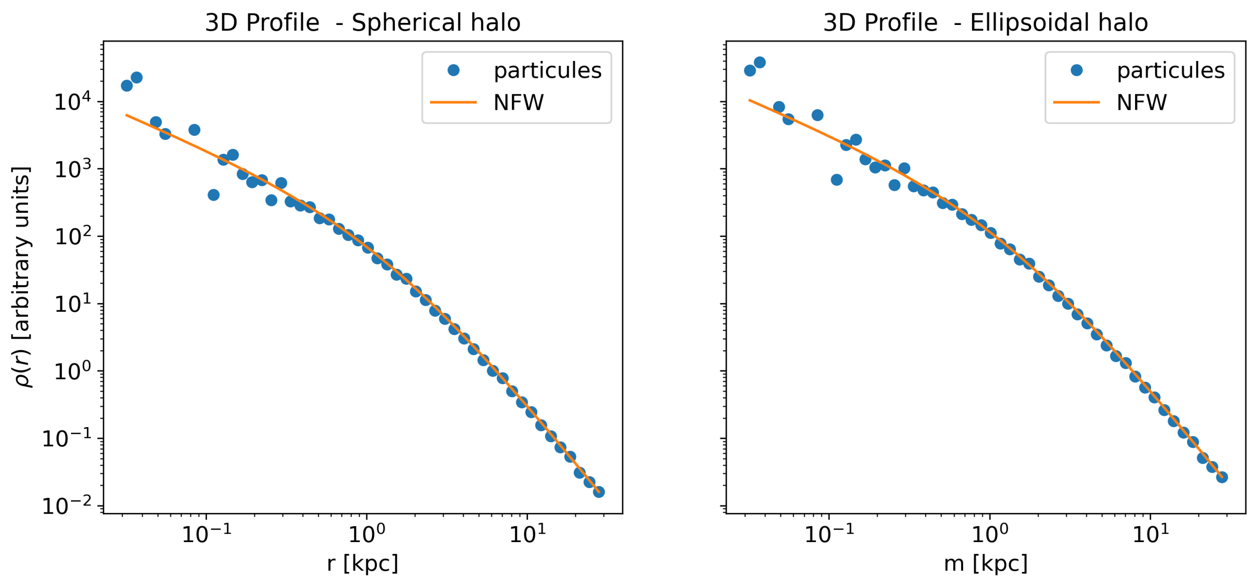

Figure 17: Validation of the artificial NFW particle sampling. The left panel shows the reconstructed three-dimensional density profile of the spherical NFW halo as a function of the spherical radius r, while the right panel shows the corresponding profile for the ellipsoidal NFW halo ($b = 0.6, c = 1.0.$) as a function of the ellipsoidal radius m. In both cases, the blue points are the density estimated from the particle distribution by counting particles in radial shells, and the orange curve is the theoretical NFW profile.